This is a postprint version of the following published document:

Effect of vertical vibration and particle size on the solids hold-up and mean bubble behavior in a pseudo-2D fluidized bed.

E. Cano-Pleite[a,*], Y. Shimizu[b], A. Acosta-Iborra[a], Y. Mawatari[b]

[a]*Department of Thermal and Fluid Engineering, Carlos III University of Madrid, Av. de la Universidad, 30, 28911, Leganés, Madrid, Spain*
[b]*Department of Applied Chemistry, Kyushu Institute of Technology, 1-1 Sensui-cho, Tobata, Kitakyushu 804-8550, Japan*

Abstract

The solids hold-up and mean bubble behavior in a vertically-vibrated fluidized bed are experimentally studied in the present work by means of Digital Image Analysis (DIA) for four different powders with Geldart classifications A, B and A/B. The bed has a small thickness (i.e. pseudo-2D bed) and operates in bubbling regime subject to a wide range of gas superficial velocities, vibration frequencies and vibration amplitudes. Mean parameters of the bed and the bubbles, such as solids hold-up, bubble fraction, bubble number density and bubble diameter and velocity, are characterized here by averaging the results over time and space. The results reveal that vibration of the bed promotes a confinement of the bubble path to the central section of the bed. This bubble confinement is more intense for the smallest particles tested and for high vibration strengths and creates two different bubble regimes in the bed. In particular, close to the distributor, the bubble velocity decreases when increasing the vibration amplitude of the bed vessel because bubbles are smaller and less confined, and they behave like isolated bubbles. The behavior of bubbles changes when they are far from the distributor, where the interaction between bubbles becomes greater due to their bigger size and the confinement of bubbles induced by vibration. This confinement promotes coalescence of bubbles. It is shown that consideration of these two different regimes of bubble dynamics allows to shed light on understanding the apparently contradictory results encountered in the literature regarding bubble behavior in bubbling vibrated fluidized beds.

Keywords: Fluidized bed, Vibration, Bubble, Pseudo-2D, DIA

1. Introduction

Fluidization is a process widely used in industry due to the good performance in solid mixing and the high gas-solid and solid-solid contact efficiencies it provides [1]. Geldart [2] proposed a classification of the powders employed in fluidization into four groups, i.e. A, B, C, D, depending on the particle diameter and

---

*Corresponding author. Tel:+34 91 624 8884
Email address: edcanop@ing.uc3m.es (E. Cano-Pleite)

density. The ease with which these powders, specially A and C, fluidize may be affected by agglomeration due to the presence of interparticle forces [2], which decreases the fluidization quality. The formation of bubble preferential paths inside the bed, that cause large heterogeneities in the particle spatial distribution, may be another effect to be avoided. Several strategies have been proposed to eliminate agglomeration and improve fluidization homogeneity. The use of mechanical stirrers in the bed, the pulsation of the gas flow [3], ferromagnetic particles subject to magnetic fields [4, 5], perturbation by acoustic fields [6], rotatory distributors [7, 8] inclined injection of gas in the bed [9], and mechanical vibration [10] are some examples of ways to enhance the fluidization quality. In this regard, mechanical vibration of fluidized beds, i.e. vibrating fluidized beds (VFB), is a promising technology consisting in introducing vibratory kinetic energy to a gas fluidized bed [10–12]. This can be easily done by applying vibration in form of an oscillatory displacement to the bed vessel, which transmits its vibration to the rest of the bed. Vibration of the bed reduces minimum fluidization velocity [13], and is a very effective technique for the fluidization of cohesive particles [14, 15], drying of granular material [16, 17] and agglomeration control [18]. Vibration with and without the injection of gas through the base of the bed can be also used to control segregation in a granular bed [19–21].

Despite its advantages, vibration substantially increases the complexity of the fluidized bed behavior and introduces new phenomena that are still not completely understood or are even unexplored. Additionally, the complexity of the system is magnified by the interaction between multiple bubbles when the bed is operating in bubbling regime. It is well-known that the performance of a fluidized bed is primary affected by the bubbling phenomenon. Therefore, as there is a need of experimental and simulation characterization of fluidized beds in general, this need is even truer for vibrating fluidized beds in bubbling regime.

Concerning experiments aimed at characterizing fluidized beds, beds of small thickness, i.e. pseudo two-dimensional beds (pseudo-2D beds), have shown to be of great importance for the understanding of fluidized beds [22–25]. This kind of bed typically has a transparent wall and possesses a small thickness, so that optical access to the system is allowed. However, in these beds, the solids motion is restricted due to the presence of the front and rear walls, which may cause different quantitative behaviors in the bed in terms of bubble diameter, rising velocity, frequency, concentration, minimum fluidization velocity, etc. [26, 27]. The use of pseudo-2D beds is also of great importance in vibrated fluidized beds because they make possible the observation of how vibration affects the bubble distribution in the bed [28] and allow for the calculation of the bubble position and diameter [29, 30]. Digital Image Analysis (DIA) is one of the most used experimental techniques aimed at understanding the bed and bubble behavior in fludized beds [22–25] and has proved to be valid also for VFBs in fluidized bed systems [12, 28–32] and for the study of the effect of vibration on bubbles present in liquid columns [33].

Existing experimental and numerical bubble studies of bubbles in VFBs are mainly centered on beds working under bubbling regime [12, 29, 31, 34–37] and beds with aggregation problems due to the utilization of fine powders [38, 39]. Global indicators such as bubble mean diameter and velocity [11, 28–31, 34], air

pressure and void fraction fluctuations [35, 36, 38], aggregate diameters [38] as well as solids circulation promoted by vibration [37] are included in these works. Some works have also investigated the effect of different vibration modes (e.g. vertical, horizontal and twist vibrations) in a fluidized bed [12, 30, 40], revealing that both vertical and horizontal vibrations change the flow patterns and the bubble behavior in the bed. However, to the authors' best knowledge, experimental studies analyzing the bubble behavior in a vertically vibrated bed still remain scarce [28–32]. The size and distribution of bubbles within a fluidized bed are of great importance for the understanding of the bed dynamics. Eccles and Mujumdar [31] studied the influence of the vessel vibration on a train of bubbles injected through a central aperture in the distributor plate and for three different kinds of particles of type A, B and D. They found that there is a resonant frequency in which the bubble diameter reaches maxima whilst the bubble velocity passes through a minimum value. Also in [31], experiments in an incipiently fluidized bed with small bubbles above the distributor were conducted using particles of 100 μm, and they revealed that the bubble diameter increases and the bubble velocity decreases when increasing the vibration frequency at a constant vibration amplitude. Zhou et al. [29, 30] measured the mean diameter and velocity of bubbles passing through two fringes of 2 cm in the upper half of a bubbling bed filled with particles of 198 μm and subject to high vibration amplitudes ($A > 5$ mm). Results in [29, 30] show that, in those fringes, both the bubble diameter and velocity increase when introducing vibration in the system. These results are in agreement with the measurements performed by Mawatari et al. [28] concerning the mean bubble velocity and diameter of bubbles in a bed filled with particles of 60 μm mean diameter. Mawatari et al. [28] also observed that, for sufficiently high vibration strengths, the flow pattern changed and that affected the bubble behavior. More recently, Cano-Pleite et al. [32] studied the behavior of isolated bubbles in a fluidized bed. They showed that the mean bubble velocity of isolated bubbles decreased when increasing the amplitude of vibration, whereas the frequency of vibration has a stronger effect on the delay of the bubble characteristics.

In all the works mentioned for bubbling regime, [28, 29, 31], the area in which the bubble behavior was quantified comprises only a fraction of the bed (i.e. a horizontal stripe of 5 cm height [28], two stripes of 2 cm height [29] and a stripe of 6 cm height in [31]), which precludes from the extraction of spatially resolved results and the determination of the variation of the bubble properties along the vertical direction. Spatially resolving the bubble behavior may shed light onto the different phenomena affecting bubble behavior and may explain in a comprehensive way the apparently contradictory trends reported in the literature [28, 29, 31, 32].

The objective of the present work is to systematically analyze and understand the bed and bubble behaviors in a vertically vibrated fluidized bed filled with four types of powders pertaining to different Geldart groups (A, A/B and B) and operating in bubbling regime over a wide range of gas superficial velocities and vibration amplitudes and frequencies. This aims at clarifying the effect of vibration on the local bubble characteristics as a function of the distance to the distributor and the resulting overall bubble behavior (i.e. averaged over the whole bed). In addition, the general bed dynamics is studied by means of

3

the bubble hold-up distribution. The results here presented reveal that vibration of the bed vessel promotes a confinement of the bubbles to the central part of the bed, especially for the bed of smaller particles. This confinement affects the way bubbles behave along the bed. In general, it is shown that the counteracting effects of i) isolated-like behavior of the bubble in the lower half of the bed and ii) vibration induced coalescence in the upper half of the bed are probably the main phenomena affecting bubble behavior in this kind of vibrated fluidized beds.

2. Experimental setup

The experimental facility used in the present work is a pseudo two-dimensional (pseudo-2D) bed of vessel dimensions 0.2 x 1.3 x 0.01 m^3 (width W, height H, and thickness K). The top section of the bed vessel is firmly attached to a vibrating structure (see Figure 1). All the vessel walls are transparent to allow optical access to the bed. Dry nitrogen (N$_2$) was employed as fluidizing gas to eliminate the moisture effect. Nevertheless, as N$_2$ properties are quite similar to those of air, no significant variation of the results would be expected if dry air were used instead of N$_2$. The nitrogen was introduced to the bed through a porous plate distributor made of sintered stainless steel with nominal filtration accuracy equal to 2 μm, which produced a uniform generation of bubbles in the lower section of the bed. The flow rate of nitrogen introduced to the bed was controlled by means of a mass flow controller, which has a resolution of 0.1 L/min ($8.3 \cdot 10^{-4}$ m/s). Particles of four different diameters were used in this work in order to investigate the effect of the particle diameter on the bubble and bed dynamics in vibrated beds. The particles were ballotini glass beads, and their mean diameter, standard deviation and density are included in Table 1. According to Geldart's classification of particles, the particles of 46.5 μm and 60 μm are of type A, those of 90.5 μm are type A/B and 120 μm particles correspond to type B. For all the experiments conducted, the bed was filled with 1.1 kg of glass beads. This corresponded to an approximate settled bed height of 0.39 m. The minimum fluidization velocity of each particle type under static conditions was measured with a pressure probe connected to the plenum. The experimental values obtained for the minimum fluidization velocity, U_{mf}, together with the theoretical values provided by Ergun's equation [41] with a void fraction of $\varepsilon = 0.4$, $U_{mf,th}$, and the gas velocity ratios, U/U_{mf}, used in the experiments are also listed in Table 1.

Table 1: Particle properties

d_p (μm)	ρ_p (kg/m^3)	U_{mf} (mm/s)	$U_{mf,th}$ (mm/s)	U/U_{mf} (-)	Geldart classification
46.5±6.5	2500	2.4	2.1	4, 8, 12, 16, 20	A
60±15	2500	3.3	3.5	4, 6, 8, 10 ,12	A
90.5±14.5	2500	9.9	7.9	2, 3, 4, 5, 6	A/B
120±15	2500	14.3	13.8	2, 2.5, 3, 3.5, 4	B

Vibration was induced in the system by means of two vibro-motors symmetrically situated at both sides of the bed (see Figure 1). Each vibro-motor had two pair of eccentric masses attached to its shaft, so that
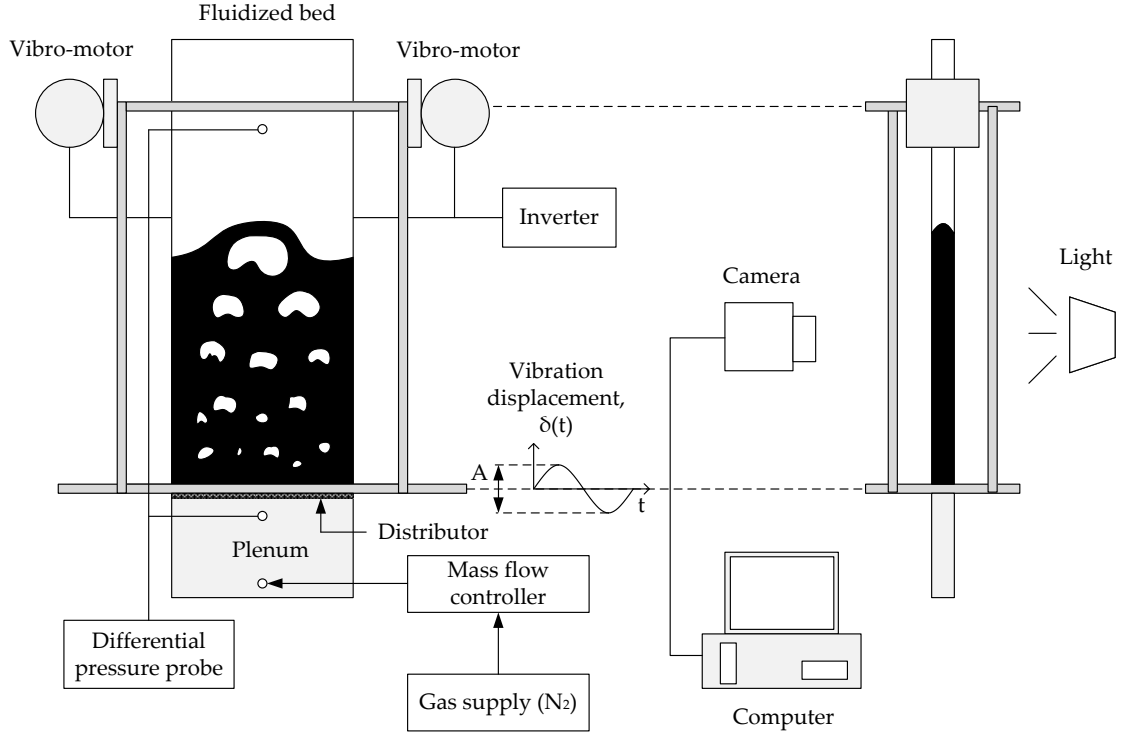
Figure 1: Experimental setup.

their rotation produced a sinusoidal displacement (vibration) of the bed vessel in the vertical direction, $\delta(t) = (A/2)\sin(2\pi f t)$. The amplitude of the vibration, A (peak-to-peak amplitude), was set by changing the relative position of the eccentric masses. The frequency of the vibration, f, was controlled by a frequency inverter that set the turning frequency of the two vibro-motors. The amplitude of the vibration was measured with a vibration meter (Showa 1332). The amplitude of vibration was also measured with DIA (Digital Image Analysis) by following the displacement of several small circular openings of the bed vessel structure, which let the light penetrate and allowed for the determination of the bed instantaneous position. The vibration meter was used to monitor the vibration amplitude of the bed vessel of the experiments, whereas DIA was employed to give a more exact figure of this vibration amplitude. It was observed that the two measures lead to results that differ very slightly.

In order to independently investigate the influence of the vessel vibration amplitude and frequency on the bed, the vibration conditions indicated in Table 2 were tested for each of the four particles sizes under study. For each kind of particle, experiments comprised three different vibration frequencies (i.e. 10, 15 and 20 Hz) keeping constant the vibration amplitude, A. This was carried out for several vibration amplitudes, including no vibration ($A = 0$), as indicated in Table 2. When the frequency of vibration of the bed vessel was changed from one experiment to another (i.e. f =10, 15 and 20 Hz for the same row in Table 2, it was

Table 2: Vibrating conditions of the experiments

d_p (μm)	f (Hz)	A (mm)	Λ (-)
		0	0
46.5	10, 15, 20	0.8±0.1	0.2-0.6
		1.9±0.2	0.4-1.5
		0	0
		0.6±0.1	0.1-0.5
60	10, 15, 20	1±0.1	0.2-0.8
		1.4±0.1	0.3-1.1
		1.9±0.3	0.4-1.5
		0	0
		0.5±0.1	0.1-0.4
90.5	10, 15, 20	0.9±0.1	0.3-0.7
		1.2±0.1	0.2-2
		1.9±0.1	0.4-1.5
		0	0
		0.6±0.1	0.1-0.5
120	10, 15, 20	1±0.1	0.2-0.8
		1.4±0.1	0.3-1.1
		2±0.2	0.4-1.6

difficult to exactly preserve the value of the amplitude of vibration A. This created a slight modification of A with the vibration frequency. To quantify this effect, Table 2 includes the mean and standard deviation of the vibration amplitude measured by means of DIA corresponding to the three vibration frequencies tested. Also, Table 2 shows the resulting intervals for the vibration strength parameter, Λ, which is the ratio of the acceleration of the vibration displacement and the gravity:

$$\Lambda = \frac{A(2\pi f)^2}{2g} \tag{1}$$

where A is the vibration amplitude, f is the vibration frequency and g is the gravity acceleration constant. In the present work, the vibration strength parameter Λ, ranges from small values to values slightly larger than $\Lambda = 1$, in order to study the effect of small strength vibrations on the bubble behavior and its dependence with the particle diameter.

The bed and bubble behavior were measured using DIA of the front section of the bed. Images were taken by a high speed CCD camera (Fastcam 1024pci). To obtain a good contrast between the bubbles and the emulsion phase, the bed was uniformly illuminated through its back wall using two spotlights, each one of 180 W. The light was able to penetrate through the bubbles, making their contours easily distinguishable from the emulsion phase. The bed was recorded by the CCD camera with a frame rate of 125 fps (for the particles of 60, 90.5 and 120 μm) and 60 fps (particles of 46.5 μm). The bed was first fluidized with nitrogen, and then vibration of the bed was produced by the vibro-motors several seconds before triggering the camera to avoid recording of start-up effects. The spatial resolution of the images was approximately 0.4 mm side

per pixel for all the cases studied. Each of the conducted experiments comprised a recording time of 51 seconds. Sensitivity analysis of the recording time, carried out by comparing the bubble behavior during the first and last 25 seconds of the experiments, showed no significant variation on bubble characteristics, which ensures a statistically stationary behavior of bubbles in the bed.

The experimental results are affected by two sources of errors. Firstly, the error related to the image analysis is caused by the discrimination of the bubble and dense phases, and is directly related to the spatial resolution and graylevel resolution of the image. The spatial resolution of the image is given by the size of a pixel, which is around $4 \cdot 10^{-4}$ m. The grayscale resolution is determined by the grayscale level, which ranges from 0 to 255, the grayscale resolution being 1. Secondly, the mean values of variables (e.g. mean bubble diameter) have an uncertainty error due to the finite size of the mean. According to the standard theory of statistics, this uncertainty of the mean of a variable is given by the standard deviation of the variable divided by the number of samples of the mean. In this work, an order of magnitude estimation of these sources of error leaded to values two orders of magnitude smaller than the variable being measured.

3. Bubble detection and processing

3.1. Bubble detection

A script in Matlab was developed for the detection and subsequent analysis of the bubble properties (i.e. bubble position and projected area). Firstly, a double thresholding methodology was applied to the raw, grayscale images to identify the dense and bubble phases. This double threshold method combines a constant and an adaptive threshold to correctly discriminate all the bubble sizes, including bubbles whose contour is not easily observable due to particle rain.

Figure 2 shows an example of the double thresholding methodology. A constant threshold based on the maximum entropy method [42] was applied to the grayscale image (Figure 2a) for distinguishing between bubble and emulsion phases (Figure 2b). Visual inspection of the images indicated that the size of bigger bubbles obtained after this first thresholding was slightly overestimated and did not capture correctly the splitting of bubbles produced by particle rain in their interior. Subsequently, a second threshold was applied to the thresholded image. This second thresholding was adaptive [43] and aimed at reducing the bubble size overestimation and improving the detection of both big and small bubbles. During the second threshold, pixels previously assigned with a value of 1 (white, dense phase) in the first threshold (Figure 2(b)) can be modified to value 0 (black, dense phase) based on the graylevel and average brightness of the surrounding pixels in a window of specified size (i.e. 30 pixels side). This improves the detection of the contours of bubbles, as shown in Figure 2(c).
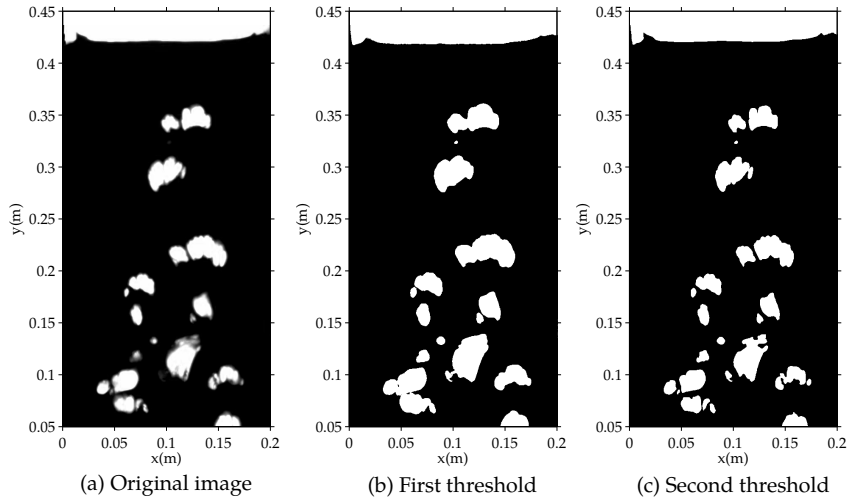
Figure 2: Snapshots of the bed. (a) Grayscale raw image taken by the CCD camera, (b) binarized image after the first (constant) threshold and (c) binarized image after the second (adaptive) threshold.

3.2. Bubble characteristics

It was found that bubbles close to the distributor were insufficiently illuminated. When approaching to the bed surface bubbles were deformed just prior eruption. Therefore, only bubbles whose centroids were within 5 to 40 cm (i.e. $\Delta h = 0.35$ m) over the distributor and have not erupted at the surface of the bed were considered for data averaging. Bubbles of area smaller than 1 cm^2 were eliminated from the analysis since their contours were not clearly distinguished. To study bubble characteristics as a function of the distance to the distributor, the bed height was divided in vertical intervals (i.e. in horizontal stripes) of 20 cm width and 2 cm height, and bubbles were assigned to an interval according to the location of their centroids.

Based on previous works [32, 44, 45], an equivalent diameter D_b of each bubble was calculated from a circle of area A_b equal to that of the bubble in the binarized images after the thresholding:

$$D_b = \sqrt{\frac{4A_b}{\pi}} \tag{2}$$

The instantaneous vertical position of a bubble, $y_b(t)$, was calculated as the vertical distance of the bubble centroid to the distributor of the bed. This position can be computed in a relative or absolute system of reference if the distance is calculated from the instantaneous or the time-averaged location of the distributor, respectively. Expressing the bubble position variation in an absolute or relative system of reference does not change significantly the mean values since the differences arising from the two reference systems are compensated when the results are time-averaged. Therefore, only results for velocities in the absolute system of reference will be presented. In order to obtain the bubble rising velocity, the vertical

8

distance between each bubble centroid in a frame, at time t, and the bubble in the following frame, at time $t + \Delta t$, was divided by the time interval between frames:

$$V_b = \frac{y_b(t + \Delta t) - y_b(t)}{\Delta t} \tag{3}$$

To avoid mismatching of bubbles in consecutive image frames and skip the perturbation of the centroid position due to bubble splitting, coalescence and break up, Equation (3) is only applied to bubbles before they split, erupt in the freeboard of the bed, or coalesce with other bubbles. Bubbles with more than 20% diameter change between consecutive frames are discarded in the analysis because they are considered to be highly perturbed by coalescence or splitting. Note that the time step between consecutive frames is $\Delta t = 8$ ms, which represents approximately a 0.5% of the total bubble residence time in the bed.

In addition to bubble size and velocity, the bubble fraction and the bubble number density were also calculated. The bubble fraction was computed as the summation of all the valid bubble areas in all the frames and the result was divided by the number of frames and the area of analysis (see Equation (4)). The bubble fraction is therefore a normalized time-averaged value of the area simultaneously occupied by the bubbles per unit area of the front view of the bed:

$$F_b = \frac{\sum_{i=1}^{N_{bub}} A_{b,i}}{N_{tot} W \Delta h} \tag{4}$$

Where $A_{b,i}$ is the bubble front area, N_{bub} is the total number of valid bubbles in all the images, N_{tot} is the total number of frames of the experiment (i.e. 6400 frames), W is the bed width and Δh is the height of the vertical interval in which F_b is calculated.

The bubble number density was calculated as the total number of valid bubbles divided by the averaging area, $W \Delta h$, and the total number of frames of the experiment:

$$n_b = \frac{\sum_{i=1}^{N_{tot}} N_{b,i}}{N_{tot} W \Delta h} \tag{5}$$

Where $N_{b,i}$ is the number of valid bubbles in the ith frame whose centroid is within a vertical interval. The definitions given in Equations (4) and (5) correspond to a vertical interval defining a thin stripe ($\Delta h = 0.02$ m), sensitivity analysis of the results to the size of the stripe thickness showed that $\Delta h = 0.02$ m is sufficient to obtain statistically significant results with a good spatial resolution in the vertical direction. Processing of consecutive intervals allows the calculation of F_b and n_b as a function of the distance to the distributor sampling areas. Also, if the sampling area approaches the whole bed ($y = 0.05 - 0.4$ m, $\Delta h = 0.35$ m) the results represent global values in all the bed.

3.3. Solids hold-up

To analyze the solids hold-up in the bed, all the grayscale images of the bed were averaged and divided by the temporal standard deviation of the grayscale images. This operation was performed individually for each pixel of the image area. The result of this operation is a normalized mean grayscale map of the distribution of solids in the bed:

$$\widetilde{GS}(i,j) = \frac{\sum\limits_{k=1}^{N_{tot}} GS(i,j)_k / N_{tot}}{\sigma_{GS}(i,j)} = \frac{\overline{GS}}{\sigma_{GS}} \tag{6}$$

Where $GS(i,j)_k$ is the grayscale image corresponding to the kth frame, i and j are the pixel location indexes in the image and N_{tot} is the total number of frames recorded by the CCD camera. In Equation (6), normalization is carried out by means of $\sigma_{GS}(i,j)$, which is the standard deviation of the variation of $GS(i,j)$ with time at a given pixel location (i,j). The normalized mean average grayscale image, $\widetilde{GS}(i,j)$ enhances the visualization of bubble paths, including those created by small bubbles, and allows for comparison between different experiments. In Equation (6), the presence of bubbles in a given pixel location (i,j) increases the mean value $\overline{GS}$. For the bed studied in this work, the values of $\widetilde{GS}(i,j)$ are typically comprised between 0 (regions with few bubble passing) and 1 (maximum bubble passing).

3.4. Bubble distribution index

The normalized mean grayscale image defined in Equation (6) provides valuable qualitative information of how bubble and dense phase are spatially distributed in the bed. However, in order perform a quantitative analysis, a distribution index of bubbles (DI) is proposed in this work. DI is calculated as the root mean square average, $\sigma_{rms,j}$, of the local standard deviation of the grayscale images within a horizontal stripe of vertical thickness $\Delta h = 2$ cm at a given distance of j pixels from the distributor. The result is normalized with the standard deviation of the local time-averaged gray level $\overline{GS}$ on this same horizontal stripe ($\sigma_{\overline{GS}_j}$):

$$DI_j = \frac{\sigma_{rms,j}}{\sigma_{\overline{GS}_j}} = \frac{\left(\frac{1}{M} \sum\limits_{i=1}^{M} \frac{1}{N_s} \sum\limits_{k=j-N_s/2}^{j+N_s/2} \sigma_{GS}^2(i,k) \right)^{1/2}}{\left[\frac{1}{M} \sum\limits_{i=1}^{M} \left(\sum\limits_{k=j-N_s/2}^{j+N_s/2} \frac{\overline{GS}(i,k)}{N_s} \right)^2 - \left(\frac{1}{M} \sum\limits_{i=1}^{M} \left(\sum\limits_{k=j-N_s/2}^{j+N_s/2} \frac{\overline{GS}(i,k)}{N_s} \right) \right)^2 \right]^{1/2}} \tag{7}$$

Where M is the number of pixels along the horizontal direction in the bed image and N_s is the number of pixels in vertical direction in the horizontal stripe of thickness Δh. If the bubble path is not well distributed in the horizontal direction, $\sigma_{rms,j}$ decreases and $\sigma_{\overline{GS}_j}$ increases, which diminishes DI_j. Thus, $DI = 0$ for a perfectly uneven distribution of bubbles in the bed (i.e. one vertical line of white pixels in the bed) and $DI \rightarrow \infty$ for a perfectly distributed bed.

4. Results and discussion

4.1. Bubble hold-up distribution

4.1.1. Solids hold-up

An important effect that vibration of the bed vessel promotes in the dynamics of the bed is the modification of the bubbles preferred paths in the bed [28], which has an impact on the bubble behavior, as will be demonstrated later in this work. As a way to qualitatively report the effect of vibration on the bubble path, Figure 3 shows the normalized mean solids hold-up (see Section 3.3) of the experiments carried out for a bed with particles of 60 μm subject to different vibration amplitudes and frequencies, and two different gas excess velocities (U/U_{mf}). Note that U_{mf} refers to the minimum fluidization velocity under static conditions, which is relatively easy to measure or to calculate using well-known correlations see Table 1.

It can be observed in Figure 3 that there exist regions in which the normalized mean grayscale image is larger than in the central section of the bed and close to the bed lateral walls. These regions typically form two easily discernible tracks that are caused because, for the bed analyzed in this work, bubbles close to the distributor follow two preferred paths that merge into a single one far from the distributor. A net upward displacement of the bed particles is induced by bubbles in the bubble path, whereas close to the walls bubbles are scarce and particles move downwards at a relatively low velocity. As can be seen in Figure 3, this downward motion region is larger if the amplitude and frequency of vibration is increased because more kinetic energy is introduced in the system and that seems to favor the flowability of the solids. Here, the bubble path is confined to the center of the bed due to the enhancement of particle circulation promoted by vibration. Also, it could be observed in the experiments that vibration promotes a larger oscillation of bubbles and a decrease of the effective U_{mf}, which contribute to coalescence and the formation of larger bubbles in the bed. Larger bubbles present in the system due to the increase of U/U_{mf} drift up a greater amount of particles through the center of the bed, and that requires a larger zone for particles to descend near to the bed walls. Confinement of the bubble path promotes the coalescence of bubbles and, as a consequence, has a significant impact on bubble characteristics such as bubble diameter and velocity.

Pairwise comparison of the normalized images in Figure 3 (e.g. Figure 3(b-c)) shows that increasing the amplitude or the frequency of vibration has a strong impact on the confinement of the bubble path. The preferred point at which bubbles coalesce can be inferred from Figure 3 as the vertical coordinate in which the two main bubble paths join in the center of the bed. This coalescence point gets closer to the distributor as the frequency and amplitude of vibration increase. It can be also observed in Figure 3 that a variation of the gas superficial velocity modifies the bubble hold-up. An increase of U/U_{mf} promotes the formation of bigger bubbles and increases the width of the bubble path. Since the increase of the gas superficial velocity promotes the formation of bigger bubbles, this also decreases the lowering of the vertical position where the

two initial paths of bubbles join.
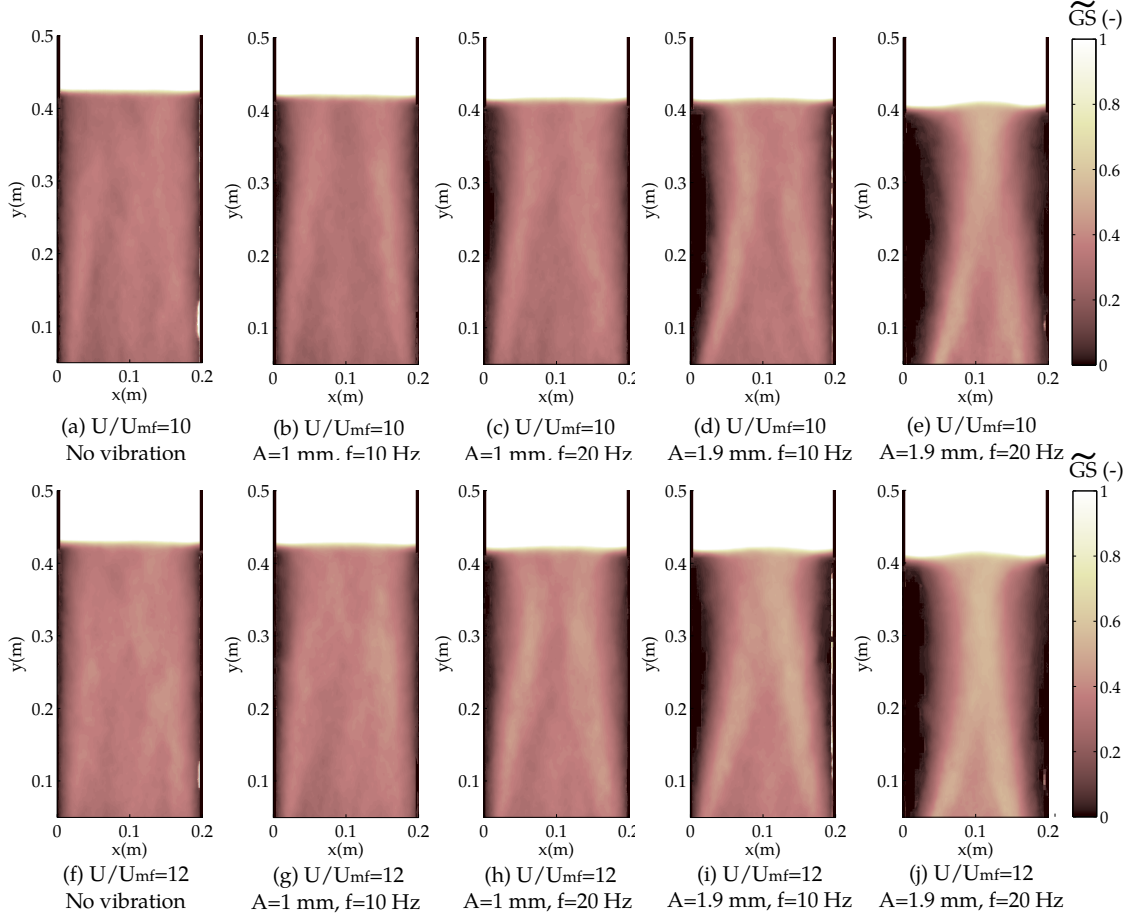
Figure 3: Normalized mean grayscale images of the bed for different vibration conditions. d_p=60 μm.

Figure 4 compares the normalized mean grayscale images for different particle sizes. Results without vibration as well as with the maximum vibration strength tested ($A = 1.9-2$ mm, $f = 20$ Hz, $\Lambda = 1.5-1.6$) are presented. For each particle size, the superficial velocity is chosen so that the gas excess velocity, $U-U_{mf}$, is similar for all the particle sizes in Figures 4(a) to (h). Note that $U - U_{mf}$ is closely related to the bubble size, which has a direct impact on the normalized mean grayscale images shown in Figures 3 and 4. On the contrary, keeping constant U/U_{mf} in Figure 4 would lead to very uneven bubble sizes among the different particles being compared. As for the particles of 60 μm in Figure 3, it can be observed in Figure 4 that bubbles tend to separate from the walls when introducing vibration in the fluidized bed regardless the particle size. From Figure 4 it seems that the impact of the vibration on the bubble path becomes more important as the particle diameter decreases. This effect is observed in Figure 4, and it can be attributed to the gulf stream circulation of particles that is promoted by vibration. The circulation of particles in the bed seems to be more intense for the smallest particles. This is attributed to their less inertia and to the smaller

proportion of particles colliding with the vibrating front and rear walls, whose oscillatory displacement may promote an increase of wall friction. As observed previously, an increase of the gulf stream motion produces a larger descending flow of particles close to the walls, which tends to confine the bubble path towards the bed center, as observed previously.
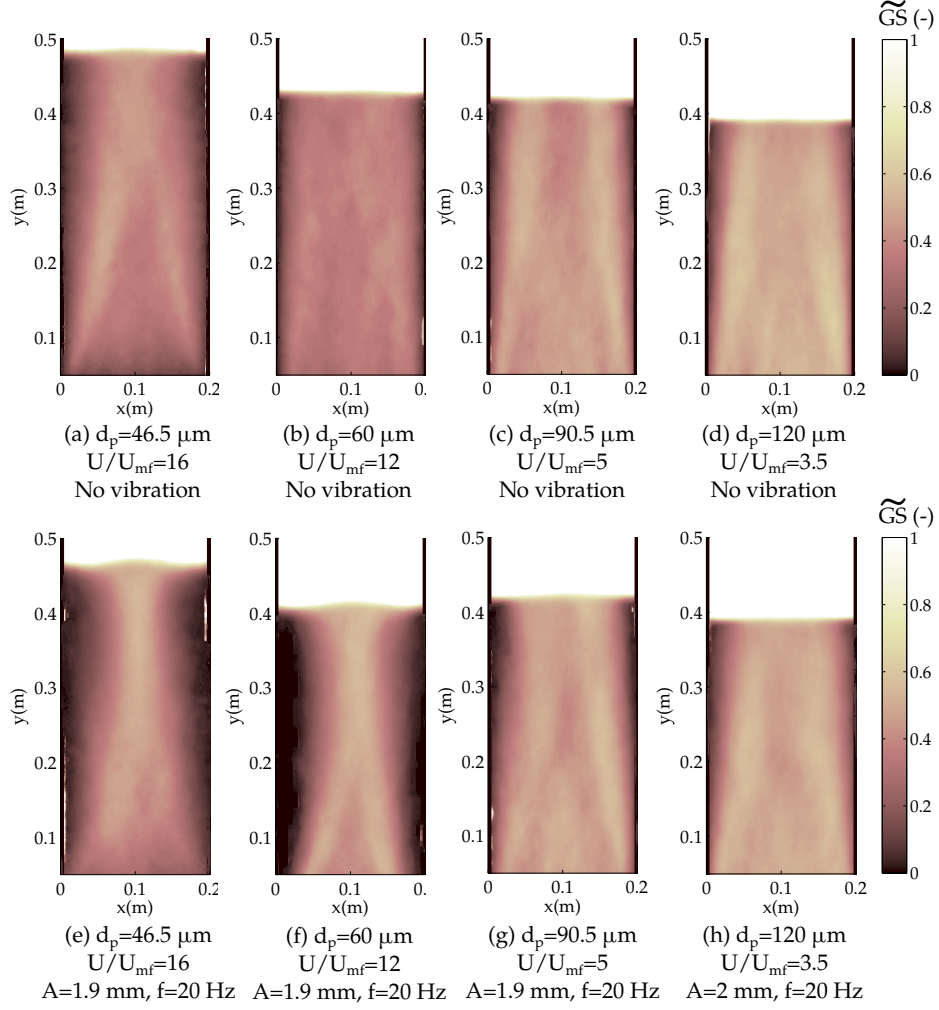
Figure 4: Normalized mean grayscale images of the bed for particles of 46.5 μm, 90.5 μm and 120 μm mean diameters: (a-d) cases without vibration and (e-h) with vibration of $A = 1.9 - 2$ mm and $f = 20$ Hz.

4.1.2. Bubble distribution index

Figure 5 shows the distribution index of bubbles in the bed (see Section 3.4) for all the particle sizes analyzed and for different vibration conditions. In Figure 5, when bubbles are uniformly distributed across the bed width, large values of the distribution index appear because bubbles induce similar values of the mean gray level in the bed along the horizontal axis and that reduces the denominator of Equation (7). Generally, excepting for the largest particles, the best distribution of bubbles along all the bed, i.e. high

distribution index, is found to be the case in which the bed is not vibrating. When introducing vibration in the system, the distribution of bubbles is less uniform and the distribution index decreases. For all the cases under study, it can be seen in Figure 5 that the distribution index decreases with the distance to the distributor because a less uniform distribution of bubbles is found due to the progressive bubble confinement to the center of the bed. For the particles of 46.5 μm and 60 μm mean diameter the variation of DI with the distance to the distributor is reduced with Λ, as bubble coalescence and the confinement of the bubble path is promoted in the lower section of the bed. The effect of the vibration of the bed vessel on the distribution index for the particles of 46.5 μm and 60 μm (Figure 5(a) and (b)) is more significant than for the particles of 90.5 μm and 120 μm (Figure 5(c) and (d)). This was also qualitatively observed in Figure 4 where the vibration-induced confinement of the bubbles to the central part of the bed with particles of 46.5 and 60 μm mean diameters (Figure 4(a, b, e, f)) was superior to the one found for particles of 90.5 and 120 μm (Figure 4(c, d, g, h)), which is attributed (see Section 4.1.1) to the larger mobility of the smallest particles in the vibrated bed, which enhances a more intense convective circulation of particles in the bed. Particles with diameter 60 μm seem to lead to a distribution index more sensitive to Λ than the other particles, which might be related to the existence of an optimum particle size and vibration strength for which the gas drag and particle inertia combine in such a way that the DI seen in Figure 5 is enhanced. More experiments would be required to give an exact answer to this phenomenon. It can be observed in Figure 5 that, in general, the distribution index decreases with the vibration strength Λ, that is, with the amplitude of the acceleration produced by vibration due to the larger confinement of bubbles to the central section of the bed. According to the Figure 5, an increase of both the amplitude and frequency of vibration of the bed vessel accentuates the progressive confinement of the bubble path with the distance to the distributor due to the enhancement of convective circulation of particles in the bed. Thus, in all the particles tested, the least uniform distribution of bubbles (i.e. minimum distribution index) appears in Figure 5 for the conditions of maximum vibration amplitude and frequency, $A = 1.9 - 2$ mm and $f = 20$ Hz.

4.2. Mean bubble characteristics

Bubble characteristics are studied in this section for beds with particles of 60, 90.5 and 120 μm mean diameters. Beds with particles of 46.5 μm mean diameter will not be considered because they produced intense particle rain inside bubbles which prevented their correct visualization and subsequent analysis. To analyze the effect of the bubble characteristics as a function of the distance to the distributor, a fixed frequency of 20 Hz (i.e. the highest vibration strengths, Λ) together with an intermediate gas excess ratio (i.e. U/U_{mf}=8, 4 and 3 for the particles of 60, 90.5 and 120 μm, respectively) were chosen as base cases for the analysis of these values. As explained in Section 3.2, spatial averaging of the bubble characteristics was performed by vertically dividing the bed in stripes of 2 cm.
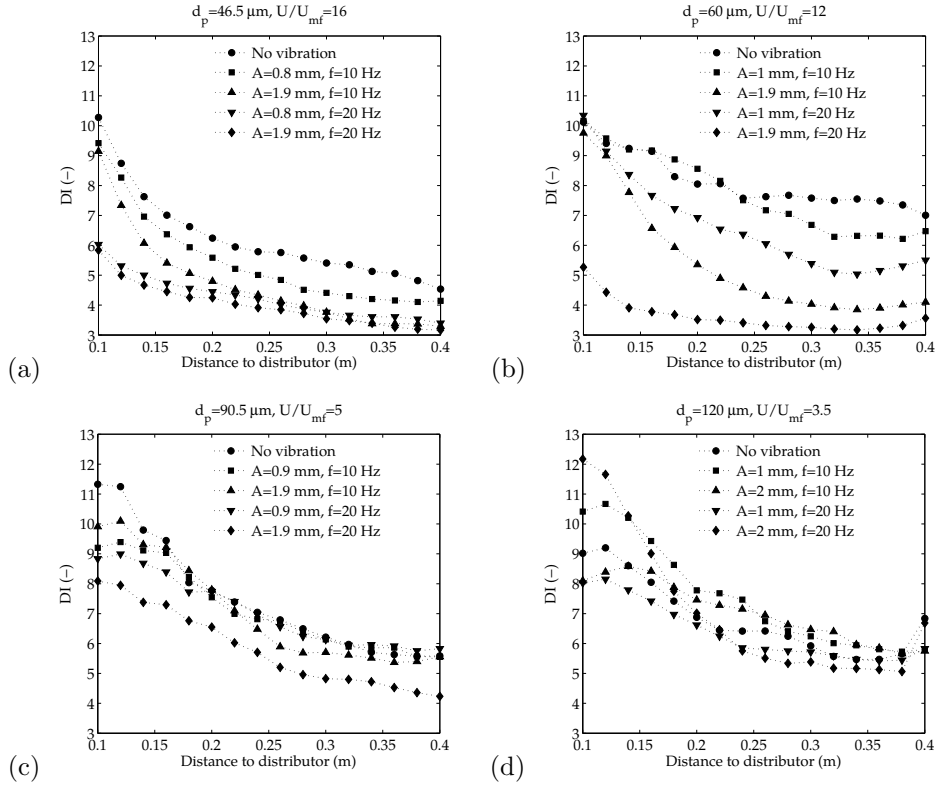
Figure 5: Distribution index as a function of the vertical distance to the distributor for different vibration strengths and mean particle diameters: (a) $d_p = 46.5$ μm, (b) $d_p = 60$ μm, (c) $d_p = 90.5$ μm and (d) $d_p = 120$ μm.

4.2.1. Bubble fraction and bubble number density

Figure 6 shows the bubble fraction (Equation (4)) and the bubble number density (Equation (5)) as a function of the distance to the distributor. It can be observed in Figure 6(a-c) that the bubble fraction increases close to the distributor and, after reaching a maximum value around $y > 0.2$ m, decreases with the vertical position. Increasing the vibration amplitude, A, produces an increase of visible flow when the bubbles are well separated, which generally happens in the lower half of the bed ($y < 0.2$ m). This tendency is reversed when bubbles are closer to each other, which occurs sufficiently far from the distributor (i.e. upper half of the bed ($y > 0.2$ m). For the particles of 60 μm, the rain of particles in bubbles may hinder the smallest bubbles located close to the distributor. Although this effect is largely reduced by means of the double thresholding methodology (see Section 2), when small particles are used the number of particles in the thickness direction is so large that their rain of particles makes difficult to capture bubbles by the high speed camera. Note that particle rain inside bubbles is always present in these kind of pseudo-2D systems [23, 25, 32]. The bubbles hindered by the rain of particles grow inside the bed until they reach a diameter big enough to be captured by the camera with accuracy, $A_b > 1$ cm^2, and that causes a growth of the bubble number density with the distance to the distributor in the lower half of the bed. Besides, the greater excess

of gas (i.e. the effective U_{mf} is reduced by vibration) produced by increasing the vibration amplitude leads to bubbles big enough to be sampled, which increases the bubble number density in the lower half of the bed for high vibration amplitudes and particles of 60 μm mean diameter. However, this is not applicable for particles of 90.5 and 120 μm since bubbles are initially big enough to be sampled. All these results suggest that there are two counteracting effects in vibration. Firstly, an increase of the vibration amplitude of the bed vessel makes bubbles bigger both by the decrease of the effective U_{mf} and by the enhancement of bubble coalescence, which promotes an increase of the number of sampled bubbles in the lower half of the bed (see Figure 6(d)) with the vibration amplitude. This is especially important for the bed of small particles, since bubbles can be more easily hindered by a curtain of particles. Secondly, vibration also promotes coalescence of bubbles when they are far enough from the distributor and that tends to increase the throughflow of gas between bubbles, which may produce a decrease of the total visible flow and the bubble number density in favor of the non-visible throughflow. In the lower half of the bed, since bubbles are more separated, the increase of bubble diameter with vibration may be the dominant mechanism affecting the visible flow. In the upper half of the bed, vibration-induced coalescence is the main effect because bubbles are bigger and closer, and thus are more prone to coalesce. All these phenomena seem to be affecting the three types of particles in Figure 6, but their separate effect is most noticeable for the smallest particles (Figure 6 (a,d)) because this bed has smaller bubbles.
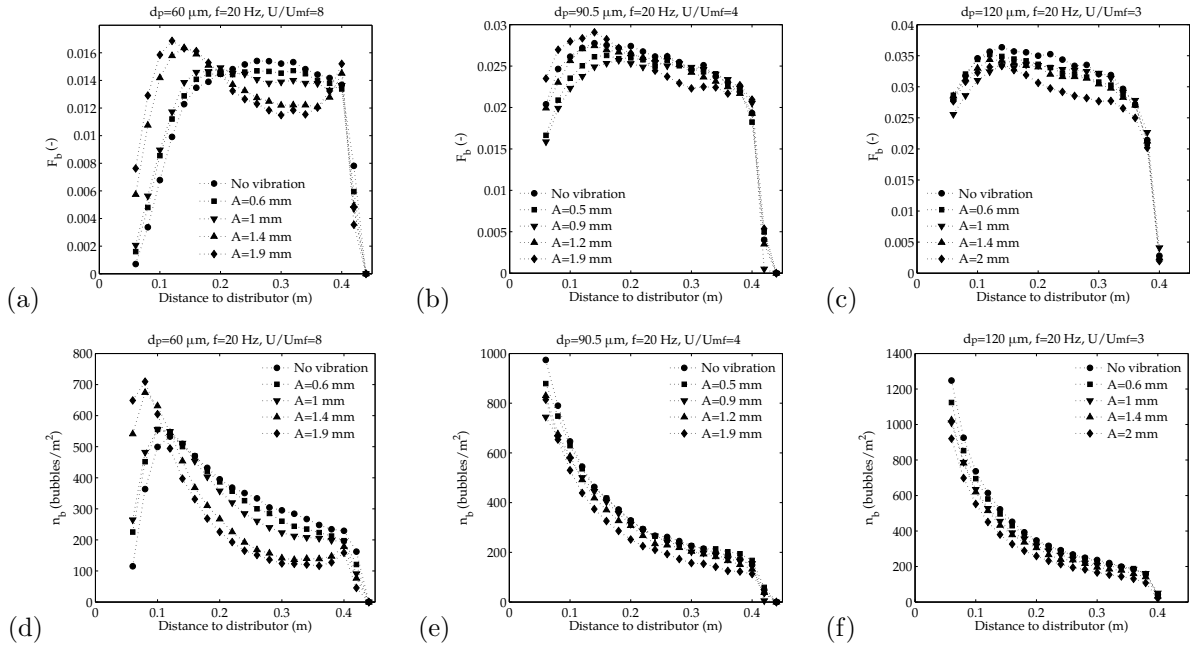
Figure 6: (a-c) Mean bubble fraction and (d-f) mean bubble number density as a function of the vertical distance to the distributor for different mean particle diameters: (a, d) $d_p = 60$ μm, (b, e) $d_p = 90.5$ μm and (c, f) $d_p = 120$ μm.

Figure 7 shows the bubble fraction covered by bubbles in the whole bed ($y = 0.05 - 0.4$ m) as a function

of the vibration amplitude for different gas velocities and vibration frequencies. In Figure 7, the bubble fraction (Section 3.2) increases with U/U_{mf}, as expected. According to the results, the bubble fraction is not very sensitive to either the vibration amplitude, A, or the frequency, f, as can be inferred from integration of Figures 7(a-c) along the bed height. In general, when introducing vibration in the system, the mean bubble diameter increases (Figure 10). At the same time, the number of bubbles is reduced as coalescence is promoted by vibration (see Figure 8). These two effects compensate and lead to small variations of the bubble fraction with the vibration amplitude and frequency. The bubble fraction increases with the particle diameter for constant values of U/U_{mf} due to the presence of bigger bubbles.
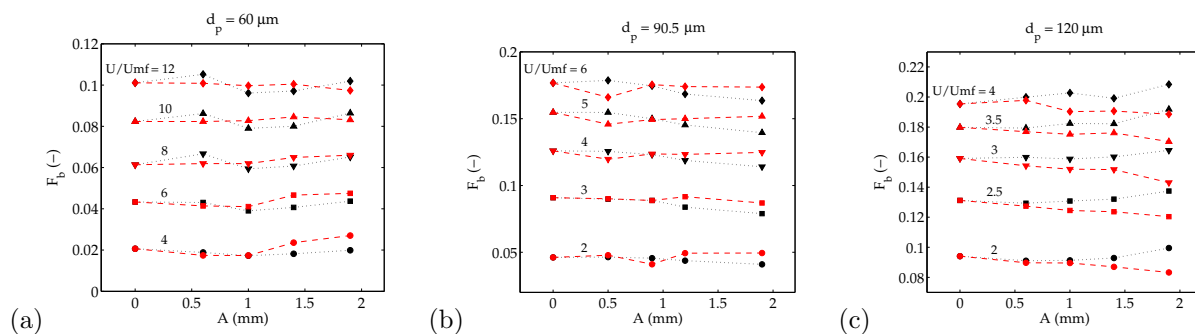
Figure 7: Mean bubble fraction as a function of the vibration amplitude for different mean particle diameters and gas superficial velocities: (a) $d_p = 60$ μm, (b) $d_p = 90.5$ μm, (c) $d_p = 120$ μm. Black symbols $f = 10$ Hz and red symbols $f = 20$ Hz.

Figures 8 shows the bubble number density in the whole bed as a function of the vibration amplitude for different vibration frequencies and superficial gas velocities. Counteracting effects are observed affecting both the bubble fraction and bubble density depending on the particle diameter. If the particles are small (60 μm), the number of bubbles increases when increasing the gas superficial velocity, because bubbles become more easily observable, as commented before. For the mean particle diameters of 90.5 and 120 μm (Figures 8(b, c, e, f)), bubbles are initially big enough to be captured and, in consequence, both an increase of U/U_{mf} and the introduction of vibration in the system promote the formation of bigger bubbles that are more prone to coalesce and that makes the mean bubble density decrease. This decrease of the mean bubble density is more pronounced at higher vibration frequencies of the bed because frequency has a strong impact on the confinement of the bubble path to the central section of the bed, as commented in Section 4.1.

4.2.2. Bubble diameter and velocity

Figure 9 shows the mean bubble diameter and vertical velocity, in an absolute system of reference, as a function of the distance to the distributor. The mean bubble diameter at any distance to the distributor, Figure 9 (a-c), increases when increasing the vibration amplitude, regardless of the effects involved (i.e. increase of isolated-like bubbles or increase due to coalescence). The mean bubble diameter decreases close

17
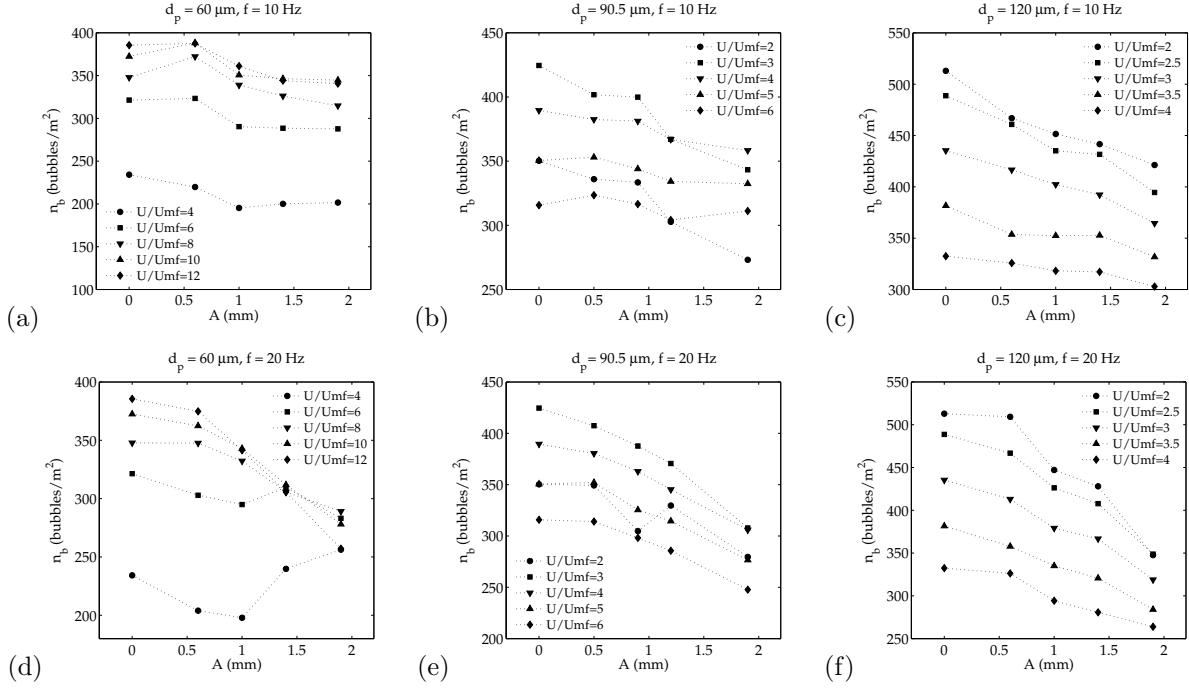
Figure 8: Mean bubble number density as a function of the vibration amplitude for different mean particle diameters and gas superficial velocities: (a, d) $d_p = 60$ μm, (b, e) $d_p = 90.5$ μm, (c, f) $d_p = 120$ μm, (a-c) $f = 10$ Hz and (d-f) $f = 20$ Hz.

to the freeboard of the bed since large bubbles are skipped from the data averaging when they are erupting at the bed surface.

The behavior of the mean bubble velocity as a function of the distance to the distributor and different vibration amplitudes is also depicted in Figure 9(d-f). Bubble absolute velocity tends to decrease with the vibration amplitude in the lower half of the bed in consonance with reported numerical predictions [34]. This decrease of bubble velocity can be explained as follows. In the lower half of the bed, bubbles are small and far enough from other bubbles so that they behave like if they were isolated bubbles (see Section 4.2.1). According to [32], the velocity of isolated bubbles decreases when the amplitude of vibration increases, which is in harmony with the behavior of the isolated-like bubbles found in Figure 9(d-f) in the lower half of the bed. On the contrary, at a sufficient distance from the distributor, i.e. the upper half of the bed, the bubble velocity tends to increase with the vibration amplitude as reported in [28–30]. This result can be understood by taking into account the confinement of the bubble path due to vibration (Figure 3). In this part of the bed, bubbles are bigger and closer to each other, and, in consequence, they tend to coalesce and their velocity becomes higher due to both the acceleration of the trailing bubble prior to coalescence with the leading bubble [1] and the larger diameter of the bubble produced after coalescence. Therefore, there is a certain distance from the distributor (about 20 cm in Figure 9) at which the dependence of the bubble velocity with vibration amplitude is reversed. For $f = 20$ Hz in Figure 9(d) the height at which the reversal

18

of tendency occurs is clearly seen. These point of inversion could be attributed to a cyclic compression and expansion of the bed bulk caused by vibration (as in [32, 44]). This may cause the bubbles in the bed to behave differently as a function of their distance to the distributor, being $y \simeq 20$ cm the region in which the trend of the bubble velocity is changed due to the confluence of these two regions, however, more experiments at different bed heights would be needed to confirm this fact. In Figures 9(e) and 9(f) this reversal of the tendency of the bubble velocity is partially hidden and is attributed to the greater buoyancy of the big bubbles present on the bed filled with particles of 90.5 μm and 120 μm, which makes them to be less affected by the vertical vibration and, in consequence, less influenced by this reversal tendency of the bubble velocity.
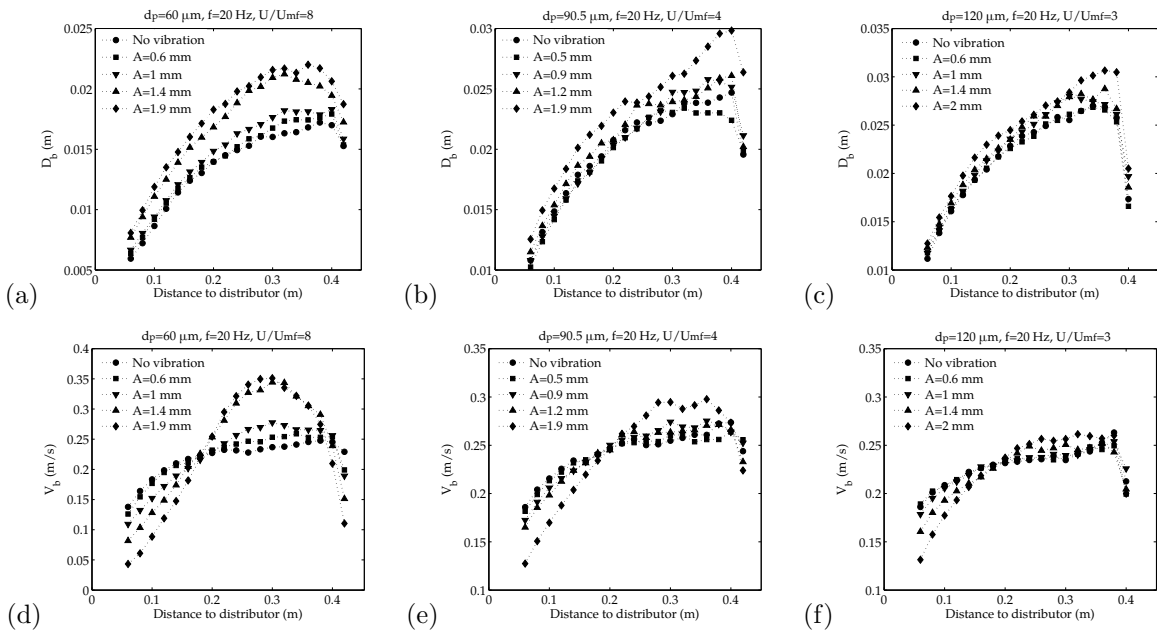
Figure 9: (a-c) Mean bubble diameter and (d-f) mean bubble absolute velocity as a function of the distance to the distributor and for different particle diameters: (a, d) $d_p = 60$ μm, (b, e) $d_p = 90.5$ μm and (c, f) $d_p = 120$ μm.

Figure 10 shows the mean bubble diameter in the whole bed for the particles of 60, 90.5 and 120 μm as a function of the vibration amplitude for different vibration frequencies and gas superficial velocities. Firstly, in Figure 10, the mean bubble diameter increases with U/U_{mf}. In the figure, generally, the bubble diameter tends to increase with the vibration amplitude due to an enhancement of coalescence. However, this is not true for the particles of 90.5 μm and a vibration frequency of 10 Hz. Two main effects may be causing this decrease of the bubble diameter. Firstly, the bubble diameter decreases due to the intense particle rain inside the bubble and the penetration of the bubble wake in the interior of the bubble, which promotes the reduction of the bubble diameter. In contrast, under the same vibration conditions, the bubbles rising in the bed of particles of 60 μm tend to drift to the central section of the bed, and that promotes bubble

coalescence and, hence, tends to enhance the increase of the bubble diameter. For these particles of 60 μm, the increase of bubble diameter due to coalescence seems to be predominant over the decrease due to the penetration of the wake in the bubble. Finally, the bed with particles of 120 μm yields to bubbles with less wake penetration and rain of particles and that seems (in view of Figure 10) to be unable to hidden the effect of the bubble growth promoted by coalescence that occurs owing to the increasing of the bed shaking when the vibration amplitude is augmented.

The increase of the mean bubble diameter with the vibration amplitude is particularly clear for the cases of high vibration frequencies combined with high U/U_{mf}, in which the mean bubble diameter grows with the amplitude of vibration while the bubble fraction remains nearly constant (Figure 7) and the mean bubble density decreases (Figure 8). This effect is more intense at high gas velocities because the resulting bubbles are bigger and closer so that bubbles are more prone to coalesce. The closeness of bubbles is also promoted by the confinement of bubbles to the central part of the bed for higher vibration strengths, as indicated in Section 4.1.
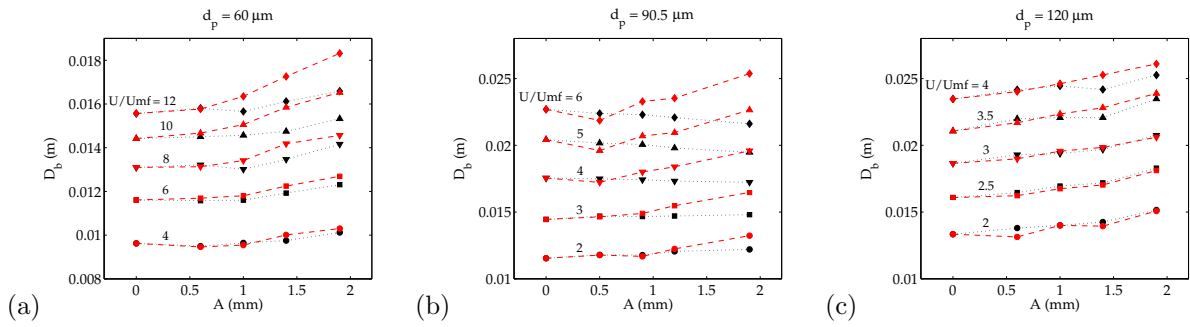
Figure 10: Mean bubble diameter as a function of the vibration amplitude for different mean particle diameters and gas superficial velocities: (a) $d_p = 60$ μm, (b) $d_p = 90.5$ μm, (c) $d_p = 120$ μm. Black symbols $f = 10$ Hz and red symbols $f = 20$ Hz.

Figure 11 shows the vertical velocity of bubbles averaged over the whole bed (i.e. bubbles within 5 to 40 cm above the distributor). In general, the average vertical velocity of bubbles decreases for $f = 20$ Hz (Figure 11(d-f)), whereas for $f = 10$ Hz it only decreases for the particles of $d_p = 60$ μm (Figure11(a)). For the particles of 60 μm and at sufficiently high U/U_{mf} and small vibration frequencies (Figure 11(a-c)) bubble absolute velocity increases with A as a consequence of the growth of the bubble diameter (Figure 10) due to both the larger excess of gas, produced by the decrease of the effective U_{mf} caused by vibration [13], and the coalescence of bubbles (Figure 8). However, in this case, the vibration strength is not enough to reduce the velocity of the bubbles except for the case $U/U_{mf} = 4$, in which the bubbles are sufficiently small to be affected by vibration as if they were an isolated bubble. Also, at small vibration frequencies, the gulf stream motion of particles drifts upwards the bubbles in the middle of the bed so that their velocity increases with the vibration amplitude. This increase of the bubble velocity with the vibration amplitude is

20

not observed in Figure 11(b, c) for the particles of 90.5 and 120 μm since their fluidization leads to bigger bubbles that are generally less affected by vibration than those in the bed with particles of 60 μm mean diameter.

Besides, in Figure 11 there is a critical value of U/U_{mf} (function of the particle size and the frequency of vibration) below which the bubble velocity decreases with the amplitude of vibration because bubbles are sufficiently small to scarcely interact with other bubbles and each bubble behaves most of the time like if it were isolated bubbles. In that case, the mean velocity of bubbles decreases with amplitude, as was justified before in Figure 9. This can be clearly observed in Figures 11(d-f). However, at higher gas velocities and vibration amplitudes, the coalescence of bubbles due to their confinement to the central section of the bed increases the velocity of bubbles and that partially counteracts the decrease of bubble velocity commented above. This results in a less significant decrease of the mean bubble velocity compared to the cases of lower gas velocities. For low vibration frequencies ($f = 10$ Hz) and particles of 90.5 and 120 μm (Figure 11(b, c)), the change of the vibration amplitude does not greatly affect the mean velocity of the bubbles.

To sum up, it can be observed in Figures 10 and 11 that both the mean bubble diameter and velocity are more sensitive to changes in the vibration amplitude for vibration frequencies of $f = 20$ Hz than for $f = 10$ Hz. Which suggests that the effect of vibration on the bed and bubble dynamics is enhanced at high vibration strengths.
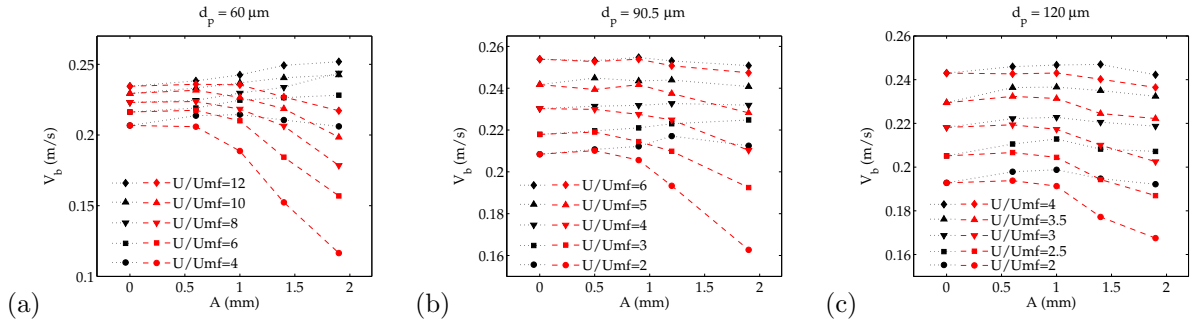
Figure 11: Mean bubble absolute velocity as a function of the vibration amplitude for different mean particle diameters and gas superficial velocities: (a) $d_p = 60$ μm, (b) $d_p = 90.5$ μm, (c) $d_p = 120$ μm. Black symbols $f = 10$ Hz and red symbols $f = 20$ Hz.

Figure 12 shows the relation between the bubble absolute velocity and diameter in the bed operated at the highest frequency tested ($f = 20$ Hz) and at an intermediate value of U/U_{mf} for the particles of 60, 90.5 and 120 μm mean diameters. Figure 12 is obtained by dividing in 20 intervals the total range of bubble diameters found in the bed and assigning the bubbles to any of the intervals depending of their diameter. Each point in Figure 12 represents the average values of bubble diameter and velocity in each interval. A clear increasing trend of the bubble velocity with the bubble diameter is observed in Figure 12 for the three types of particles under study and the vibration amplitudes tested. Accordingly with previous

reports [1], for conventional fluidized beds, the bubble velocity is proportional to the square root of the bubble diameter. This is true for the cases of no vibration in Figure 12. However, this trend changes when introducing vibration in the system and a nearly linear trend of bubble velocity with bubble diameter is observed in Figure 12 in the lower half of the bed.

Also, Figure 12 clearly shows that, for small bubbles, the bubble velocity decreases with the amplitude of vibration for a given diameter of bubble and keeping constant the gas superficial velocity. Generally, large bubbles (i.e. $D_b > 0.03$ m) are much less affected by the bed vessel vibration than small bubbles and present velocities that are even similar to those obtained without vibrating the bed. Also, these large bubbles are typically located in the upper half of the bed, where bubbles tend to coalesce and are deformed prior to their eruption, which explains why bubble velocity is more disperse in Figure 12 for $D_b \gtrsim 0.05$ m.
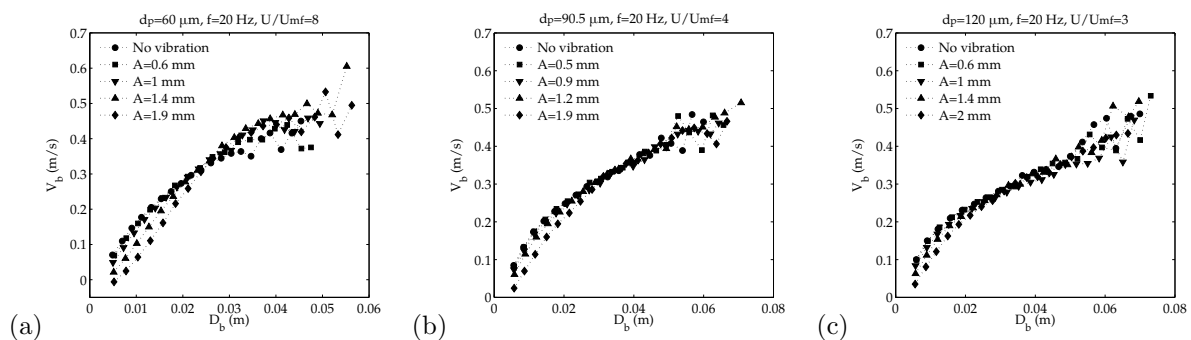
Figure 12: Mean bubble absolute velocity as a function of the mean bubble diameter for a vibration frequency $f = 20$ Hz and different vibration amplitudes and particle diameters: (a) $d_p = 60$ μm, (b) $d_p = 90.5$ μm, (c) $d_p = 120$ μm.

Alternatively, Figure 13 shows the relation between the absolute velocity and diameter of bubbles averaged in all the bed (i.e. $y = 0.05 - 0.4$ m). Each curve in Figure 13 contains 5 points that are taken from Figures 10 and 11 at a given vibration amplitude, A, for 5 different values of U/U_{mf}. Figure 13 also includes results for an intermediate vibration frequency ($f = 15$ Hz). The solid lines in Figure 13 connect data points with the same vibration amplitude, whereas the dotted lines are obtained after fitting of the points having the same superficial velocity and are included to facilitate the visual inspection of the results. Therefore, the increase of bubble size in Figure 13 from left to right is principally caused by the increase of U/U_{mf} and not by bubble coalescence as a function of the distance to the distributor. That explains why the slope of the curves does not decay for large bubble diameters as in Figure 12. Thus, the results depicted in Figure 13 reflect the global behavior of bubbles in the bed, and each point corresponds to an individual experiment.

There are three effects affecting the bubble velocity in vibration that have been observed in previous figures and can be used to understand Figure 13. Firstly, if the bubble is sufficiently separated from other bubbles and the vibration strength is high (i.e. higher frequency of vibration) it behaves as if it was an

isolated bubble due to the scarce interaction with the surrounding bubbles. In this situation, an increase of vibration amplitude produces a decrease of bubble velocity, for a given bubble size, as commented before when Figure 12 was analyzed and previous works with isolated bubbles [32, 44]. This effect causes that at high vibration frequencies, e.g. Figure 13(c,f,i), the mean bubble velocity in the bed clearly decreases when increasing the vibration amplitude for a given superficial velocity ratio U/U_{mf}, this promotes a negative slope of the dashed lines in Figure 13 (c,f,i). This slope decreases when increasing the gas superficial velocity, which indicates that the velocity of larger bubbles (due to the higher U/U_{mf}) is less affected by the vibration amplitude than for smaller bubbles. The bubble velocity decrease with vibration amplitude is still observed, to a lesser extent, at intermediate frequencies on all the particle sizes (i.e. $f = 15$ Hz, Figures 13(b,e,h)), and at low frequencies and the larger particle diameter ($d_p = 120$ μm). As can be seen in the left hand side of Figure 13, the decrease of bubble velocity with A is more significant for lower superficial velocities, for which bubbles are smaller and interaction between bubbles is still reduced.

Secondly, on passing from no vibration to vibration, the mean bubble diameter grows due to a decrease of the effective U_{mf} (as seen in Figure 10). This effect is also observed in Figure 13 in which D_b decreases with A for a given U/U_{mf}. Exception of this is Figure 13(d) for large values of U/U_{mf} where the experimental points are very close and the effect of A is unclear. Thirdly, as seen in Section 4.1, vibration of the bed vessel produces recirculation of particles in the bed, creating a net upward motion of particles in the center of the bed whereas by the walls the motion of particles is downwards. This upward motion of particles is higher if gas superficial velocities or the amplitude of vibration are increased because more kinetic energy is introduced in the system [37]. Owing to the upward motion of particles, bubbles tend to be faster because they are normally confined to the central section of the bed and they interact more with each other [28–30], and, in consequence, bubbles cease to behave as if they were isolated. The increase of the interaction of bubbles, together with the growth of bubbles due to coalescence tends to increase the bubble velocity, as seen in Section 4.2.2, and this occurs when bubbles are sufficiently far from the distributor. For example, in Figure 13(a) an increase of vibration amplitude promotes a growth of the bubble velocity due to the presence of bigger bubbles and the confinement of the bubble path to the central section of the bed (see also Figure 11(a)). In this situation the velocity of bubbles is mainly affected by confinement, coalescence and diameter growth because the vibration frequency is small in contrast to Figure 13(c,f,g) where the vibration frequency is high. In the case of particles of intermediate diameter, $d_p = 90.5$ μm, and low vibration frequency, $f = 10$ Hz, no clear trend is found for bubble velocity because probably the confinement of the bubble path and bubble coalescence are competing against the commented effect of the amplitude of vibration. It is clear from Figure 13 that adequate selection of vibration amplitude and frequency can be used to influence and have some control on the bubble behavior for a given particle size and gas superficial velocity.
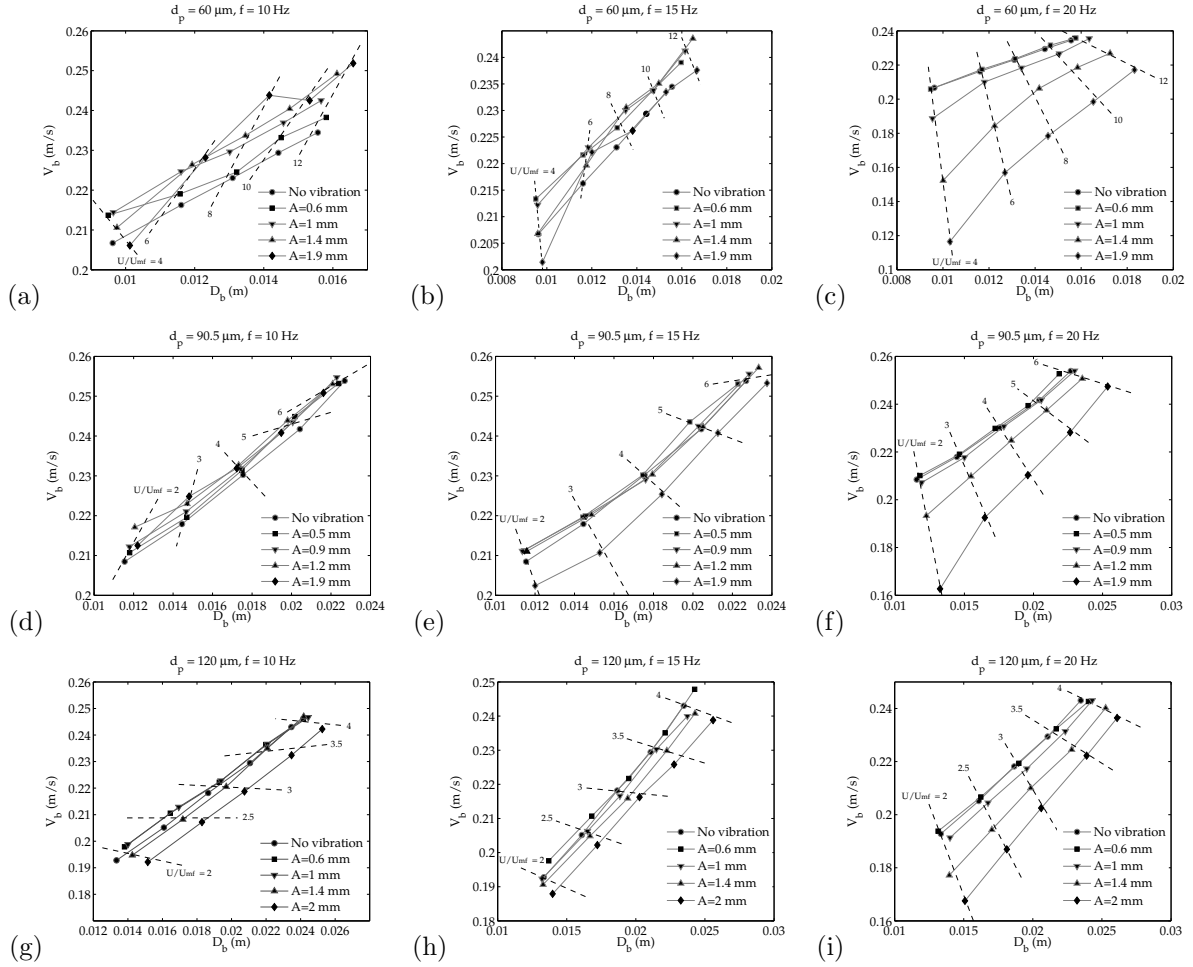
Figure 13: Mean bubble velocity as a function of the mean bubble diameter for different vibration amplitudes and frequencies. The gas superficial velocity increases from left to right in each curve. (a-c) d_p =60 μm, (d-f) d_p = 90.5 μm, (g-i) d_p = 120 μm.

5. Conclusions

The solids hold-up and mean bubble behaviors in a vertically vibrated fluidized bed were experimentally studied in the present work by means of DIA. Experiments with four different sizes of particles at several vibration strengths were carried out in order to obtain a wide range of results regarding bubble and bed dynamics. The analysis of results covered different aspects to show, and help to understand, the multiple effects of vibration on the bed and bubble dynamics.

Firstly, mean characteristics of the bed were studied by averaging over time and space the solids hold-up. The mean solids hold-up allowed the characterization of the bubble distribution inside the bed. The experiments revealed that, when introducing vibration in the system, the bubble path tends to be confined to the center of the studied bed, making the distribution of bubbles less uniform. The confinement of the bubble path is more significant when increasing the vibration strength. The bubble number density in the bed

24

decreases with an increase of vibration amplitude due to bubble coalescence whereas the bubble fraction remains nearly constant. In general, the vibration amplitude has an impact on the mean diameter and velocity of bubbles that is greater at high vibration frequencies. In the bubbling bed tested, increasing the vibration amplitude produces an increase of the mean bubble diameter, specially at high vibration frequencies. Two regimes of bubble dynamics were detected in the bed, depending on the vibration characteristics, the particles employed and the bed morphology. Small bubbles close to the distributor (i.e. lower half of the bed) were found to behave more similarly to isolated bubbles, so that their velocity decreased when increasing the vibration amplitude. In contrast, the bubble velocity increased with the vibration amplitude for bubbles in the upper half of the bed, as they were more influenced by bubble coalescence and gulf stream drifting of particles. In summary, all the previous results show that careful selection of the vibration amplitude and frequency, altogether with the gas velocities and type of particles, may be used to modify the bed behavior, including the number, size and velocity of bubbles in the bed. Also, bubbles behave differently depending on their spatial location in the bed and this may explain the different, and apparently contradictory, trends found in the literature concerning the bubble behavior in vibrated fluidized beds.

Nomenclature

A = vibration amplitude, peak-to-peak (mm)

A_b = bubble area (m^2)

D_b = bubble equivalent diameter (m)

DI = distribution index (-)

d_p = particle diameter (μm)

f = vibration frequency (Hz)

F_b = bubble fraction (-)

GS = grayscale value (-)

$\overline{GS}$ = mean grayscale value (-)

$\widetilde{GS}$ = normalized mean grayscale value (-)

g = gravity acceleration constant (m/s^2)

H = bed vessel height (m)

Δh = height of a sampling area in the bed (m)

K = bed thickness (m)

M = number of pixels in the horizontal dimension (-)

n_b = bubble number density (bubbles/m^2)

N_{bub} = number of bubbles (-)

N_s = number of vertical pixels in a stripe (-)

N_{tot} = total number of frames of a experiment (-)

t = time (s)

U = gas superficial velocity (m/s)

U_{mf} = minimum fluidization velocity (m/s)

V_b = bubble velocity (m/s)

$\overline{V}_b$ = averaged V_b (m/s)

W = bed width (m)

y = vertical coordinate (m)

y_b = bubble centroid vertical coordinate (m)

Greek letters

$\delta(t)$ = bed vessel vertical displacement (m)

Λ = vibration strength parameter (-)

ρ_p = particle density (kg/m^3)

σ = standard deviation

Acknowledgments

References

[1] D. Kunii, O. Levenspiel, Fluidization Engineering: Butterworth-Heinemann: Newton, MA, 1991.

[2] D. Geldart, Types of gas fluidization, Powder Technol. 7 (1973) 285.

[3] S.A. Sadiq, M. Asif, Fluidization of nano-powders: Effect of flow pulsation, Powder Technol. 225 (2012) 86-92.

[4] R.E. Rosenweig, Fluidization: hydrodynamic stabilization with a magnetic field, Science 204 (1979) 57-60.

[5] G.N. Jovanovic and Z.R. Jovanovic, Bubble size and fluidization regimes in magnetically controlled fluidized beds, paper no. 28i. AIChE Annual Meeting, St. Louis, MO, U.S.A. (1993).

[6] W. Nowak, M. Hasatani, M. Derczynski, Fluidization and heat transfer of fine particles in an acoustic field, AIChE Symp. Ser. 89 (1993) 137-149.

[7] C. Sobrino, J.A. Almendros-Ibáez, D. Santana, M. de Vega, Fluidization of Group B particles with a rotating distributor, Powder Technol. 181 (2008) 273-280.

[8] J. Gómez-Hernández, A. Soria-Verdugo, J. Villa Briongos, D. Santana, Fludized bed with a rotating distributor operated under defluidization conditions, Chem. Eng. J., 195-196 (2012) 198-207.

[9] H. Nakamura, T. Kondo, S. Watano, Improvement of particle mixing and fluidization quality in rotating fluidized bed by inclined injection of fluidizing air, Chem. Eng. Sci. 91 (2013) 70-78.

[10] R. Gupta, A.S. Mujumdar, Aerodynamics of a vibrated fluid bed, Can. J. Chem. Eng. 58 (1980) 332-338.

[11] K. Noda, Y. Mawatari, S. Uchida, Flow patterns of fine particles in a vibrated fluidized bed under atmospheric or reduce pressure, Powder Technol. 99 (1998) 11-14.

[12] T. Zhou, H. Kage, S. Funaoka, H. Ogura, Y. Matsuno, Fluidization behaviour of glass beads under different vibration modules, Adv. Powder Technol. 12 (2001) 559-575.

[13] Y. Mawatari, Y. Tatemoto, K. Noda, Prediction of minimum fluidization velocity for vibrated fluidized bed, Powder Technol. 131 (2003) 66-70.

[14] N.J.M Kuipers, E.J. Stamhuis, A.A.C.M. Beenackers, Fluidization of potato starch in a stirred vibrated fluidized bed, Chem. Eng. Sci. 51 (1996) 2727-2732.

[15] Y. Mawatari, M. Tsunekawa, Y. Tatemoto, K. Noda, Favorable vibrated fluidization conditions for cohesive fine particles, Powder Technol. 154 (2005a) 54-60.

[16] A.S. Mujumbar, Handbook of Industrial Drying. Marcel Dekker. New York, 1987.

[17] C. Strumillo, Z. Pakowski, Drying of granular products in vibrofluidized beds, in: A.S. Mujumdar (Ed.), Drying'80: Developments in Drying, Hemisphere Publishing Corporation, Montreal, (1980) 211-226.

[18] C. Xu, J. Zhu, Experimental and theoretical study of the agglomeration arising from fluidization of cohesive particles-effects of mechanical vibration, Chem. Eng. Sci. 60 (2005) 6529-6541.

[19] Y. Nahmad−Molinari, G. Canul−Chay, J.C. Ruiz−Suárez, Inertia in the Brazil nut effect, Phys. Rev. E 68 (2003) 041301.

[20] J. Sun, F. Battaglia, S. Subramaniam, Dynamics and structures of segregation in a dense, vibrating granular bed, Phys. Rev. E 74 (2006) 1-13.

[21] X. Yang, Y. Zhao, Z. Luo, S. Song, C. Duan, L. Dong, Fine coal dry cleaning using a vibrated gas-fluidized bed, Fuel Process. Technol. 106 (2013) 338-343.

[22] J.A. Laverman, I. Roghair, M. van Sint Annaland, Kuipers, H., Investigation into the hydrodynamics of gas-solid fluidized beds using particle image velocimetry coupled with digital image analysis, Can. J. Chem. Eng. 86 (2008) 523-535.

[23] A. Busciglio, G. Vella, G. Micale, L. Rizzuti, Analysis of the bubbling behaviour of 2D gas solid fluidized beds: Part I. Digital image analysis technique, Chem. Eng. J. 140 (2008) 398-413.

[24] F. Hernández-Jiménez, S. Sánchez-Delgado, A. Gómez-García, A. Acosta-Iborra, Comparison between two-fluid model simulations and particle image analysis & velocimetry (PIV) results for a two-dimensional gas-solid fluidized bed, Chem. Eng. Sci. 66 (2011) 3753-3772.

[25] L. Shen, F. Johnsson, B. Leckner, Digital image analysis of hydrodynamics two-dimensional bubbling fluidized beds, Chem. Eng. Sci. 59 (2004) 2607-2617.

[26] D. Geldart, The size and frequency of bubbles in two- and three-dimensional gas fluidised beds, Powder Technol. 4 (1970) 41-55.

[27] R.R. Cranfield, D. Geldart, Large particle fluidisation, Chem. Eng. Sci. 29 (1974) 935-947.

[28] Y. Mawatari, K. Tagawa, Y. Tatemoto, K. Noda, Bubbling characteristics under vertical vibration in a two-dimensional fluidized bed, Chem. Eng. Jpn. 38 (2005b) 18-23.

[29] T. Zhou, H. Kage, H. Li, Bubble characteristics in a two-dimensional vertically vibro-fluidized bed, China Partic. 3 (2005) 224-228.

[30] T. Zhou, H. Ogura, M. Yamamura, H. Kage Bubble motion pattern and rise velocity in two-dimensional horizontal and vertical vibro-fluidized beds, Can. J. Chem. Eng, 82 (2004) 236-242.

[31] E.R.A. Eccles and A.S. Mujumdar, Bubble phenomena in aerated vibrated beds of small particles, Drying Technol. 15:1 (1997) 95-116.

[32] E. Cano-Pleite, F. Hernández-Jiménez, M. de Vega, A. Acosta-Iborra, Experimental study on the motion of isolated bubbles in a vertically vibrated fluidized bed, Chem. Eng. J., 255 (2014) 114-125.

[33] T. O'Hern, B. Shelden, J. Torczynsky, L. Romero, Bubble oscillations and motion under vibration, Phys. Fluids 24 (2012)

091108.

[34] A. Acosta-Iborra, F. Hernández-Jiménez, M. de Vega, J.V. Briongos, A novel metodology for simulating vibrated fluidized beds using two-fluid models, Chem. Eng. J. 198-199 (2012) 261-274.

[35] L. Xiang, W. Shuyan, L. Huilin, L. Goudong, C. Juhui, L. Yikun, Numerical simulation of particle motion in vibrated fluidized beds, Powder Technol. 197 (2010) 25-35.

[36] Y. Tatemoto, Y. Mawatari, T. Yasukawa, K. Noda, Numerical simulation of particle motion in vibrated fluidized bed, Chem. Eng. Sci. 59 (2004) 437-447.

[37] C. Zeilstra, M.A. van der Hoef, J.A.M. Kuipers, Experimental and numerical study of solids circulation in gas-vibro fluidized beds, Powder Technol. 248 (2013) 153-160.

[38] D. Barletta, M. Poletto, Aggregation phenomena in fluidization of cohesive powders assisted by mechanical vibrations, Powder Technol. 225 (2012) 93-100.

[39] D. Barletta, G. Donsi, G. Ferrari, M. Poletto, P. Russo, The effect of mechanical vibration on gas fluidization of a fine aeratable powder, Chem. Eng. Res. Des. 86 (2008) 359-369.

[40] Y. Mawatari, T. Koide, Y. Tatemoto, T. Takeshita, K. Noda, Comparison of three vibrational modes (twist, vertical and horizontal) for fluidization of fine particles, Adv. Powder Technol. 2 (2001) 157-168.

[41] S. Ergun, Fluid flow through packed columns, Chem. Eng. Prog. 48 (1952).

[42] J.N. Kapur, P.K. Sahoo, A.K. Wong, A new method for gray-level picture thresholding using the entropy of the histogram, Comput. Graphics Image Process. 29 (1985) 273285.

[43] D. Bradley and G. Roth, Adaptive thresholding using the integral image, Journal of Graphics Tools 12:2 (2007) 1321.

[44] E. Cano-Pleite, F. Hernndez-Jimnez, A. Acosta-Iborra, Compressible-gas two-fluid modeling of isolated bubbles in a vertically vibrated fluidized bed and comparison with experiments, Chem. Eng. J. 271 (2015) 287-299.

[45] F. Hernández-Jiménez, A. Gómez-García, D. Santana, A. Acosta-Iborra, Gas interchange between bubble and emulsion phases in a 2D fluidized bed as revealed by two-fluid model simulations, Chem. Eng. J. 215-216 (2013) 479-490.

[46] T. Akiyama, K.M. Aoki, K. Yamamoto, T. Yoshikawa, Experimental study on vibration-induced convection and heaping in granular beds, Granul. Matter 1 (1998) 1520.